



Active Tectonics of the Nantinghe Fault in Southeastern Tibetan Plateau and its Implications for Continental Collision

Feng Shi^{1,2*}, Honglin He^{1,2}, Yiduo Liu³, Zhanyu Wei^{1,2} and Haoyue Sun^{1,2}

¹State Key Laboratory of Earthquake Dynamics, Institute of Geology, China Earthquake Administration, Beijing, China, ²Shanxi Taiyuan Continental Rift Dynamics National Observation and Research Station, Beijing, China, ³Department of Earth and Atmospheric Sciences, University of Houston, Houston, TX, United States

Quantifying the structure and kinematics of active faults is the key to understanding the India-Eurasia continental collision. While the boundary faults of blocks in the southeastern Tibetan Plateau region have been under scrutiny for decades, relatively less attention has been paid to the active faults within the blocks. Here, we use structural, sedimentary, and geomorphic characteristics to constrain the late Quaternary kinematics and slip rates of the Nantinghe fault, a major fault within the southeastern Tibetan Plateau region. The Nantinghe fault is an active, dominantly left-lateral strike-slip fault that can be traced continuously for 500 km. We analyze the late Quaternary slip rates at five sites along the fault trace. The latest Quaternary apparent throw rates are typically less than 1 mm/a. The rate of strike-slip displacement is estimated to be an order of magnitude higher, 4.0 ± 0.6 (2σ) mm/a. Trenching suggests that active fault behavior is dominated by strike-slip faulting and reveals five earthquake events with refined information of timing in the last 5,000 years, suggesting an averaged recurrence interval of $\sim 1,000$ a. These observations agree with GPS-derived estimates and show that late Quaternary slip rates on the Nantinghe fault are comparable to those on other major active strike-slip faults in the southeastern Tibetan Plateau. The newly-obtained slip rates on the Nantinghe fault, integrated with previous estimates on other faults in this region, provide direct evidence that favors the continuum models over the rigid block ones, on the Quaternary deformation mechanism in the India-Asia continental collision.

Keywords: Southeastern Tibetan plateau, nantinghe fault, late quaternary, active faulting, slip rates, India-Asia collision

1 INTRODUCTION

The Indian-Asian continental collision during the past ca. 50 Myr has induced crustal deformation in a vast region that extends more than 2,000 km from the Himalaya Mountains to Central and East Asia (Molnar and Tapponnier, 1975; Royden et al., 2008; Taylor and Yin, 2009). Two end-member views dominate the debates on continental collision dynamics: 1) block models, in which intercontinental deformation is concentrated on major faults that separate a number of relatively rigid blocks (Dewey et al., 1973; Avouac and Tapponnier, 1993; Peltzer and Saucier, 1996; Tapponnier et al., 2001; Meade, 2007; Thatcher, 2007); and 2) continuum models, in which

OPEN ACCESS

Edited by:

Wenjun Zheng,
Sun Yat-sen University Zhuhai
Campus, China

Reviewed by:

Hu Wang,
Southwest Jiaotong University, China
Bo Zhang,
Peking University, China

*Correspondence:

Feng Shi
shifeng@ies.ac.cn

Specialty section:

This article was submitted to
Structural Geology and Tectonics,
a section of the journal
Frontiers in Earth Science

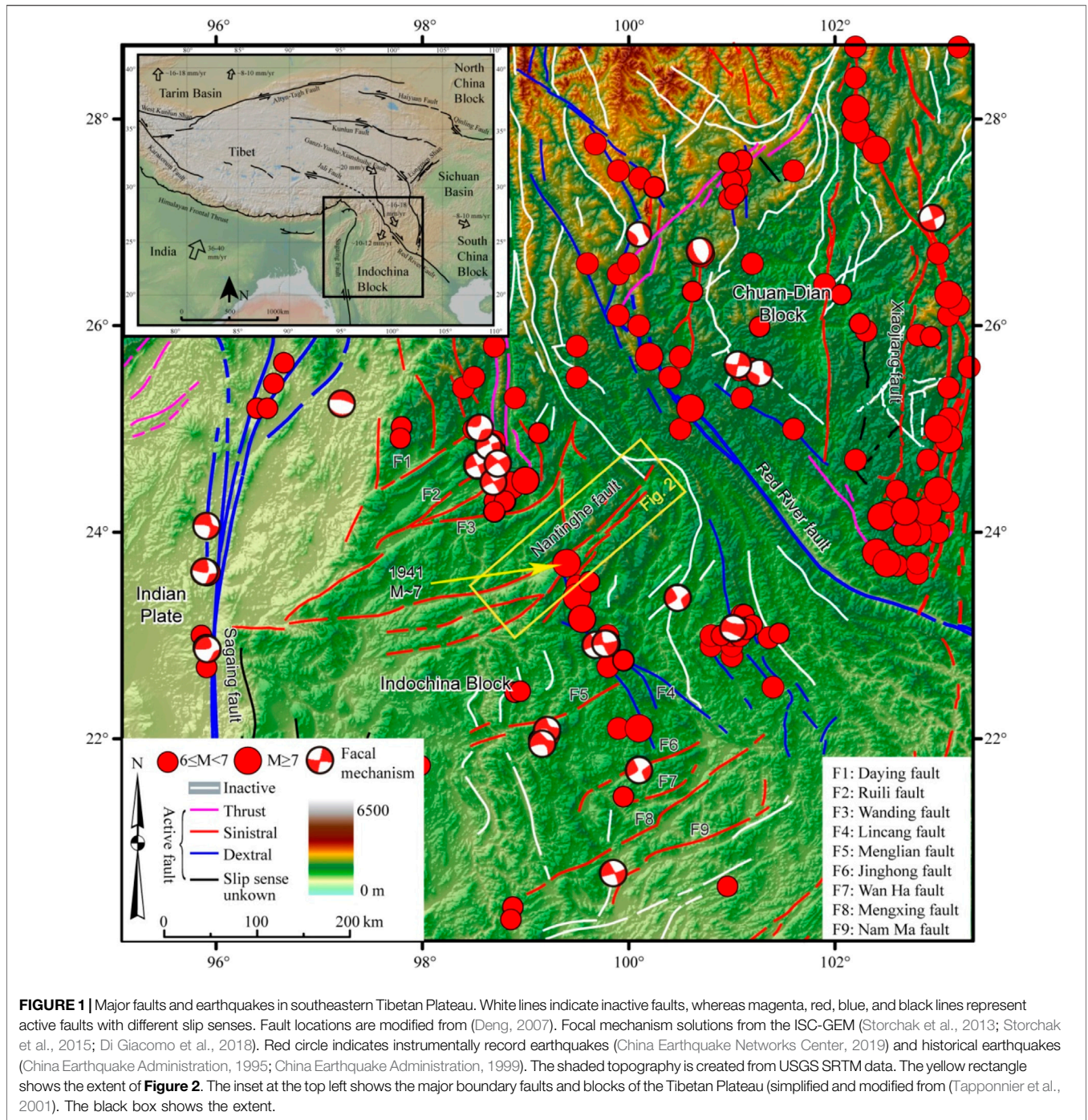
Received: 19 November 2021

Accepted: 29 December 2021

Published: 21 January 2022

Citation:

Shi F, He H, Liu Y, Wei Z and Sun H
(2022) Active Tectonics of the
Nantinghe Fault in Southeastern
Tibetan Plateau and its Implications for
Continental Collision.
Front. Earth Sci. 9:818225.
doi: 10.3389/feart.2021.818225



deformation is regionally distributed in the shallow brittle crust, and is essentially continuous at depth (Molnar and Tapponnier, 1975; England and McKenzie, 1982; England and Houseman, 1986; Clark and Royden, 2000). When these two schools of view are applied to eastern Asia, large slip rates on major faults are required by the block models, but not by the continuum models. In general, the block models predict large slip rates (mostly over 10 mm/a (Tapponnier et al., 2001; Thatcher, 2007) on the major faults between tectonics blocks and small or negligible slip rates

(far less than the slip rates on the major faults between tectonic blocks (Lacassin et al., 1998; Tapponnier et al., 2001; Thatcher, 2007) on the faults within the blocks. The continuum models, in contrast, do not imply such a difference, and the predicted slip rates are all around or less than 5 mm/a (England and Molnar, 2005).

The southeastern Tibetan Plateau, including the Indochina Block and the Chuan-Dian Block, is a natural laboratory to assess this debate (Tapponnier et al., 2001) (**Figure 1**). The block models

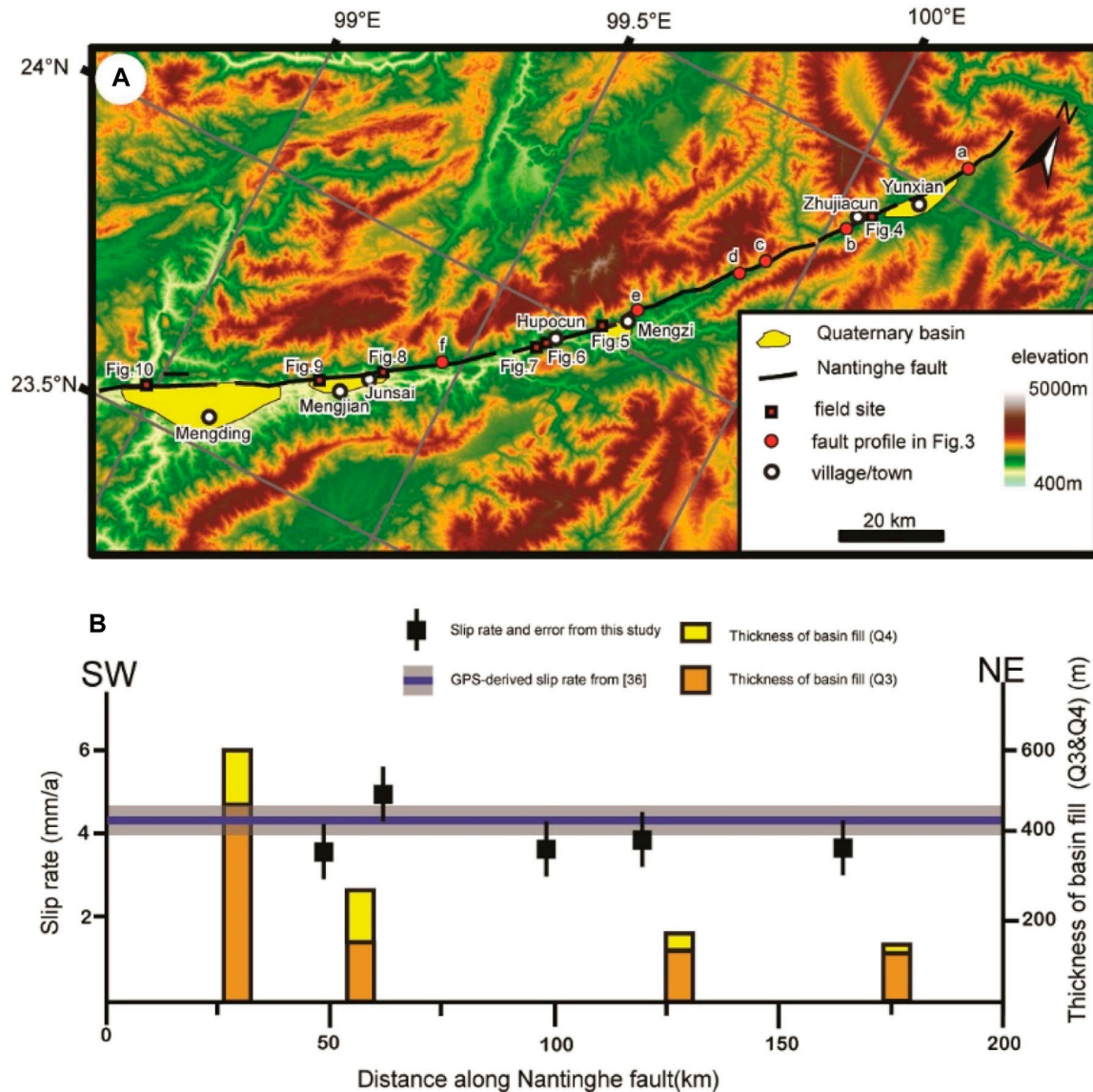
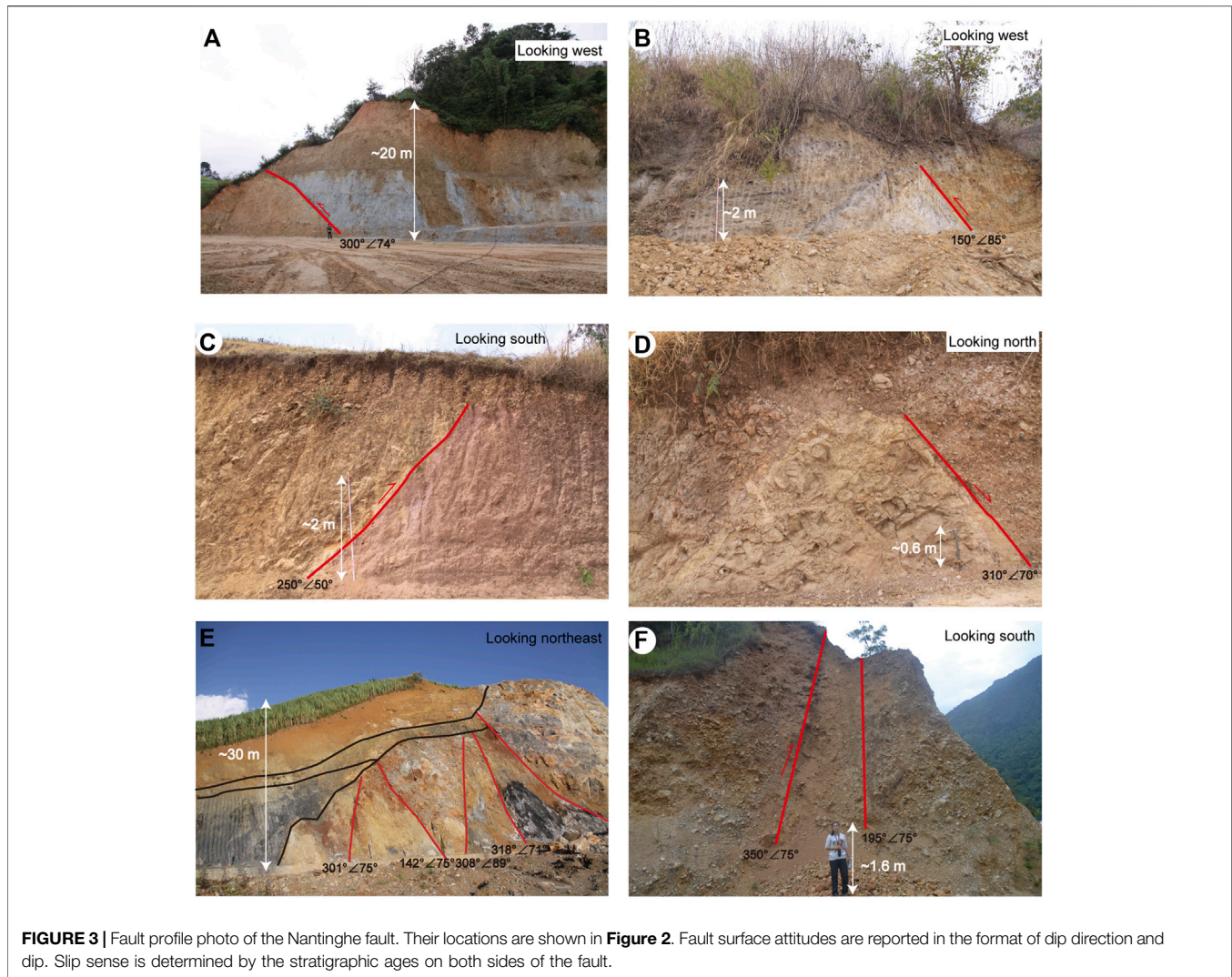


FIGURE 2 | (A) Fault map of the active Nantinghe fault. **(B)**, strike-slip rates and depth of basin along the Nantinghe fault. Blue line with shadows is strike-slip rates and errors estimated from GPS surveys (Wang, 2009). Black squares with black line are strike-slip rates and error bars estimated in this study. Orange rectangle is the thickness of the older basin fill (Q3), yellow rectangle is the thickness of the younger basin fill (Q4).

suggested that the boundary fault, Ailao Shan-Red River shear zone or Red River fault, dominates the extrusion of the Indochina block during the past 40 Myr, and predicted that the slip rates of the strike-slip faults (e.g., Daying, Ruili, Nantinghe, Mengxing, among others) within the Indochina block should be substantially lower than that of the Red River fault (Lacassin et al., 1998). In contrast, in the continuum models, although the Red River fault forms a striking geomorphic feature, it does not dominate the present-day kinematics of the whole block, and the slip rates of the internal faults may be comparable with, or even greater than, that of the Red River fault (Copley, 2008). Because of their obvious geomorphic features, fast slip rates, and the occurrence of devastating earthquakes, the block-bounding

Red River and Sagaing faults have attracted intensive investigations (Allen et al., 1984; Tapponnier et al., 1990; Weldon et al., 1994; Leloup et al., 1995; Wang et al., 1998; He et al., 2002; Shen et al., 2005; Leloup et al., 2007; He and Oguchi, 2008; Wang et al., 2014; Shi et al., 2016; Shi et al., 2018a). In contrast, a lesser amount of attention has been paid to the active faults within the blocks. Seismic station networks and historical documents have recorded numerous earthquakes with magnitudes greater than 6 within the block (China Earthquake Administration, 1995; China Earthquake Administration, 1999; China Earthquake Networks Center, 2019). GPS measurements and geomorphic analysis also indicated that the interior of the Indochina Block is actively deforming (Copley, 2008; Wang et al.,



2014; Shi et al., 2018b). However, to our knowledge, some faults within the Indochina Block remain enigmatic in terms of their slip rates and the timing and recurrence interval of paleoearthquakes during the Quaternary. This makes it difficult to quantify the kinematics and seismicity of the block deformation, and hence hinders the evaluation of the dynamics of continental collision in the southeastern Tibetan Plateau region.

In this study, we choose the Nantinghe fault, the largest one within the Indochina Block, to assess its activity and testify the competing models. While the GPS-derived sinistral strike-slip rate of the Nantinghe fault (~ 4 mm/a) (Wang, 2009) is close to the field- and GPS-derived sinistral strike-slip rate of the Red River fault (~ 5 mm/a) from decades to tens of thousands years (Allen et al., 1984; Weldon et al., 1994) or even larger than the slip rate of the Red River fault (~ 1 mm/a) from stratigraphic and geomorphologic investigations over the last 30,000–50,000 years (Shi et al., 2018a), how fast it slipped at a greater time scale is still unknown. We focus on the northeastern 200 km of the Nantinghe

fault zone (**Figure 2**). This is because 1) geological evidence is more extensively exposed along the northeastern portion of the fault zone, and 2) the southwestern portion of the fault in Myanmar is relatively inaccessible. We adopt a combination of techniques, including field mapping, image interpretation, surveying of offset geomorphic markers, and trenching, in order to elucidate the history of fault slip over the last few thousand years, and to fill a gap in the paleoearthquake records in this forestry and remote area.

2 GEOLOGICAL SETTING

The Indochina Block lies in the southeast of the Tibetan Plateau. It is bounded by two major strike-slip boundaries, the Red River fault to the east and the Sagaing fault to the west (**Figure 1**). Many strike-slip faults cut the region between these faults, forming rugged terrain whose elevation ranges from 500 to 3,000 m. Most

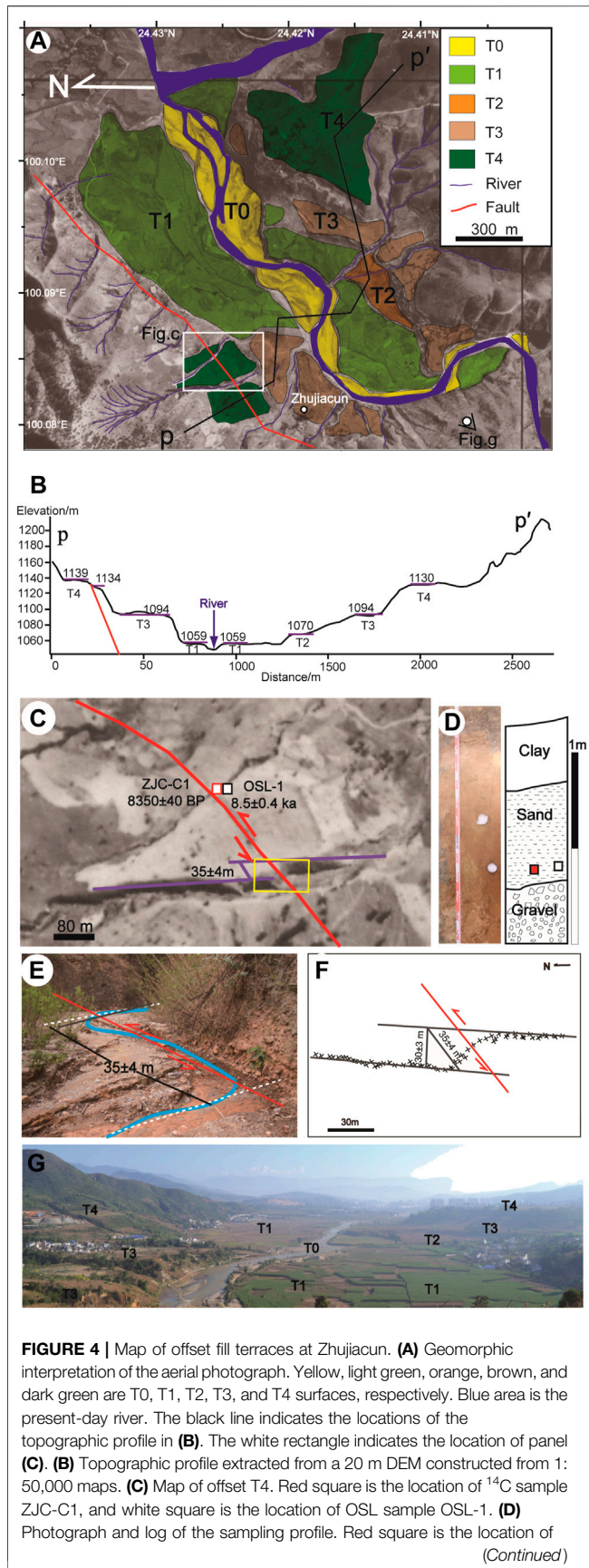


FIGURE 4 | the ^{14}C sample, and white square is the location of the OSL sample. **(E)** Photograph of the offset, view to NW. **(F)** Map of offset, obtain from differential GPS measuring system. Cross symbol shows the measured location of the river. **(G)**, Photograph of terraces, viewing to the northeast.

of these faults strike NE-SW and have arc-shaped surface traces. The Indochina Block moved southeastward relative to the Eurasian plate as an extrusion body along the sinistral strike-slip Ailaoshan-Red River shear zone, and the dextral strike-slip Red River fault during the early stage (between ca. 35 and 17 Ma) of the India-Eurasia collision (Tapponnier et al., 1990; Leloup et al., 1995; Leloup et al., 2007). As the Indian plate continued moving north, an inversion occurred in the Indochina block, switching from east-west compression to east-west extensions. Slip sense on the Red River fault changed to right-lateral before at least 5 Ma (Leloup et al., 2007) or even 8–20 Ma (Wang et al., 2016; Wang et al., 2019; Wang et al., 2020).

As one important fault within the Indochina Block, the Nantinghe fault initiated at the end of the early Paleozoic and was reactivated in different geological periods (Huang and Ren, 1987). Slip sense on the Nantinghe fault that changed to left-lateral is associated with slip sense on the Red River fault that changed to right-lateral (Lacassin et al., 1998). The eastern tip of the Nantinghe fault zone is located northwest of Yunxian County, Yunnan Province, SW China. It extends westward through Mengzhi, Mengjian, Mengding towns in Yunnan, China into Shan State in eastern Myanmar. Where it is detectable on the surface, the fault appears to dip 70–85°NW in the northeastern segment and 70–80°SE in the southwestern segment (Shi, 2014).

Exposures of the active Nantinghe fault show that it coincides with zones of dense fracturing in Pre-Quaternary bedrocks; the width of these zones is generally ~10–50 m but can be occasionally up to a few hundred meters. In remote sensing imagery, strands of the fault form clear linear features associated with scarps, shutter ridges, and offset drainages, characteristic of active strike-slip deformation. The fault movement is dominated by left-lateral strike-slip, with minor net vertical slip (Shi, 2014). Previous estimates of the fault activity vary, especially on the northern segment (Zhu et al., 1994; Wang et al., 2006; Sun et al., 2017). Moreover, some parameters of activity, such as slip rates of all fault and the paleoearthquake events of south segments, are still poorly constrained for the Nantinghe fault.

3 METHODS AND TECHNIQUES

3.1 Fault Mapping

We mapped the active traces of the Nantinghe fault zone (**Figure 2**) using the Advanced Land Observation Satellite (ALOS) imagery (2.5 m spatial resolution) and Chinese aerial photographs (~1 m spatial resolution) (Chen et al., 2006). We then carried out field observations at sites with geomorphic indicators of late Quaternary activity, including scarps or offset surfaces in Quaternary deposits, offset channels, shutter ridges, and linear valleys (**Figure 3**). Offset landforms were

TABLE 1 | Optically stimulated luminescence (OSL) data and ages.

Sample	Site name	Counts/ks	K ₂ O (%)	Total dose rate (Gy/ka)	Equivalent dose (Gy)	Age (Ka)
OSL-1	Zhujiacun	12.1 ± 0.4	1.66	3.7 ± 0.2	31.6 ± 0.9	8.5 ± 0.4
OSL-2	Daxueshan	9.2 ± 0.3	1.42	3.0 ± 0.2	5.5 ± 0.1	1.8 ± 0.1
OSL-3	Hupocun	12.6 ± 0.4	2.16	4.2 ± 0.2	55.7 ± 2.1	13.2 ± 0.7
OSL-4	Junsai	5.6 ± 0.2	0.80	1.8 ± 0.1	24.5 ± 0.8	13.3 ± 0.5
OSL-5	Mengjia	8.3 ± 0.3	0.92	2.4 ± 0.1	9.0 ± 0.2	3.7 ± 0.2
OSL-6	Mengding	8.5 ± 0.4	1.23	3.3 ± 0.2	3.6 ± 0.2	1.1 ± 0.1

Note: All sample preparation and analyses were conducted by the State Key Laboratory of Earthquake Dynamics, China. See detail in the **Supplemental Material**.

TABLE 2 | Radiocarbon sample information and analytical results.

Sample	Material	Radiocarbon age	13C/12C ratio	2σ Calendar age
ZJC-C1	Charcoal	8350 ± 40 BP	-25.9‰	7522–7328 BC
HPTC-C1	Charcoal	520 ± 40 BP	-18.7‰	1315–1356 BC (21.3%) 1388–1448 BC (74.1%)
MDTC-C5	Charcoal	4970 ± 40 BP	-26.0‰	3929–3877 BC (9.8%) 3804–3654 BC (84.6%)
MDTC-C17	Charcoal	1710 ± 30 BP	-27.2‰	251–697 AD
MDTC-C38	Charcoal	690 ± 30 BP	-26.2‰	1265–1312 AD (68.9%) 1358–1366 AD (26.5%)

Note: All sample preparation and analyses were conducted by Beta Analytic Inc. All samples were analyzed using accelerator mass spectrometry. All raw radiocarbon ages were calibrated by OxCal 4.3 (Bronk Ramsey, 2009). The calibration calculates probability distributions for raw radiocarbon ages with associated uncertainties (reported by the lab facility). Radiocarbon ages BP, relative to 1950. All samples typically underwent the acid-alkali-acid (AAA) method before radiocarbon dating.

surveyed using a differential GPS (DGPS) measuring system, with a measurement repeatability of finer than ±10 cm. For some large-scale offsets, we estimated it from the ALOS imagery and aerial photographs beside the field survey.

The majority of the evidence for active faulting came from offset or truncated fluvial fill terraces. Fill terraces in this region are typically composed of subhorizontal, crudely- to well-bedded gravel and sand layers. We identified terrace surfaces and assigned relative ages based on the relative height between the surface and the modern river bed. At each site, terraces were numbered in ascending order from the youngest (T0, representing the modern channel bed) to the oldest. We further determined absolute ages of fill terrace deposition and abandonment using ¹⁴C and optically stimulated luminescence (OSL) dating techniques on samples from the sand layers (Aitken, 1998). The ¹⁴C analysis is performed in the Beta Analytic Radiocarbon Dating Laboratory. The raw radiocarbon ages are calibrated by OxCal 4.3 (Bronk Ramsey, 2009). The OSL dating is conducted in the State Key Laboratory of Earthquake Dynamics. We did not obtain sufficient evidence to assess whether terrace ages can be correlated between different sites along the Nantinghe fault, or whether the terrace chronology is site-specific.

While the strike-slip component prevails along the entire fault, along-strike variations exist in terms of the ratios of strike-slip and dip-slip components as well as the strike-slip rates. We describe our observations below in both horizontal and vertical offsets. Throw rates are relatively small (less than

1 mm/a) along each fault segment, and the ratio of strike-slip and dip-slip components varies.

3.2 Trenching

To document the timing of recent slips on the fault, we excavated two trenches across the Nantinghe fault at two sites. Accurate location of fault traces and sufficient sediment accumulation with organic materials are two key factors for trenching. In Mengding township (**Figure 2**), we established a site that is located at a well-developed fault trough valley on an alluvial fan and excavated a 2-m-deep trench across the fault. The steep terrain south of the site has trapped sediment, providing abundant organic materials. To assess possible differences in fault activity between different segments, we excavated another 2-m-deep trench across the fault at Hupocun township (**Figure 2**). This site is also located on an alluvial fan surface. The steep terrain to the north of the site provides sufficient sediment accumulation and organic materials. All trench walls were cleaned and logged at a scale of 1:10 following standard procedures (McCalpin, 1996). Depositional ages of the units in the trench facies were provided by ¹⁴C analysis of charcoal fragments and OSL analysis on sands.

4 RESULTS

The Nantinghe fault can be traced continuously for approximately 200 km in Yunnan Province, SW China. The fault shows clear evidence for Quaternary sinistral strike-slip displacement, with minor components of dip slip. Field-based

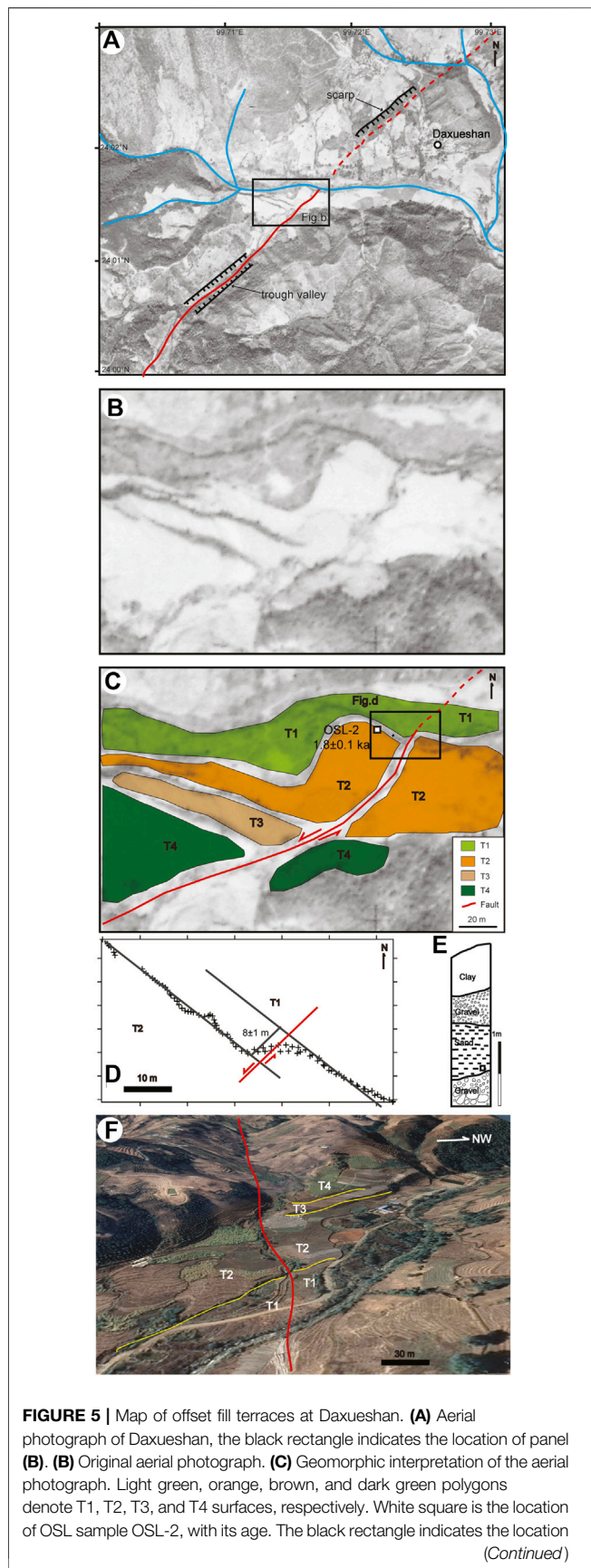


FIGURE 5 | of panel **(D)**. **(D)**, Map of offset T1/T2 riser, obtain from differential GPS measuring system. Cross symbol shows the measured location of the T1/T2 riser. **(E)**, Log of the sampling profile. Black square shows the location of the sample OSL-2. **(F)**, Geomorphic interpretation of the Google Earth images, in oblique view with no vertical exaggeration. Location: 24.0234°N, 99.7165°E. Viewing southwest. Red curve denotes the surface trace of the Nantinghe fault.

geology data, especially fault profiles, are key to identifying fault traces. Several fault profiles (**Figure 2**) and their tectonic geomorphology characteristics form the pieces of evidence of fault traces along the Nantinghe fault. Below we document the results from northeast to southwest along the fault.

4.1 Zhujiacun

Zhujiacun is located southwest of Yunxian county. Offsets of fill terraces at this site are clearly shown on aerial photographs (**Figure 4**). We then mapped these terraces in the field investigations. Fill terraces are typically composed of subhorizontal, crudely- to well-bedded gravel and sand layers. We identified five terrace surfaces (T0, T1, T2, T3, and T4) based on the relative height between the surface and the modern river bed (**Figure 4B**). The fault has caused a sinistral offset to the gully of T4 by approximately 35 m, and a vertical offset of the T4 surface by 5 m. The ages of T4 were estimated at 8.5 ± 0.4 ka based on our OSL dating and 8350 B.P. based on ^{14}C dating (**Tables 1, 2**). Both methods yield a similar age, indicating the age of T4 is ca. 8.5 ka. Based on the sinistral strike-slip displacement of the gully of T4, the vertical offset of the T4 surface, and the age of T4, we estimated the mean sinistral-slip rate of 4.1 ± 0.4 mm/a and the throw rate of ~ 0.6 mm/a. This is a minimum estimate of the strike-slip rate because the gully formed after any of the T4 sediments were deposited. No other clear terrace offsets are preserved at this site.

4.2 Daxueshan

Daxueshan is located on the southwestern margin of the Mengzi basin, about 60 km southwest of Yunxian County (**Figure 2**). Immediately south of this site, a trough valley is present, indicative of the Nantinghe fault trace in the Pre-Quaternary bedrocks (**Figure 5**). At this site, four terraces T1-T4 are all cut by the Nantinghe fault. The vertical dislocation between the hanging wall and the footwall is 5 m on the T3 terrace and 1 m on the T2 terrace, but no vertical displacement is observed on T1. The T2/T1 terrace riser is offset in a sinistral sense. Because of the twists and turns of the T3/T2 riser, it is difficult to measure accurately the sinistral offset of the T3/T2 riser.

We used the sinistral offsets of the T2/T1 riser and the T2 age to evaluate the sinistral-slip rate, and the throw rate was constrained from the height of the scarp on T2 and the T2 age. The sinistral and vertical offsets, as obtained from DGPS surveys, are 8 and 1 m, respectively. The ages of T2 at this site are 1.8 ± 0.1 ka based on OSL dating on sample OSL-2 (**Table 1**), thereby the sinistral-slip rate and the throw rate are 4.5 ± 0.8 mm/a and 0.5 ± 0.1 mm/a, respectively. Again, this is a minimum estimate of the slip rate because the riser could only form after the T2 sediments were deposited.

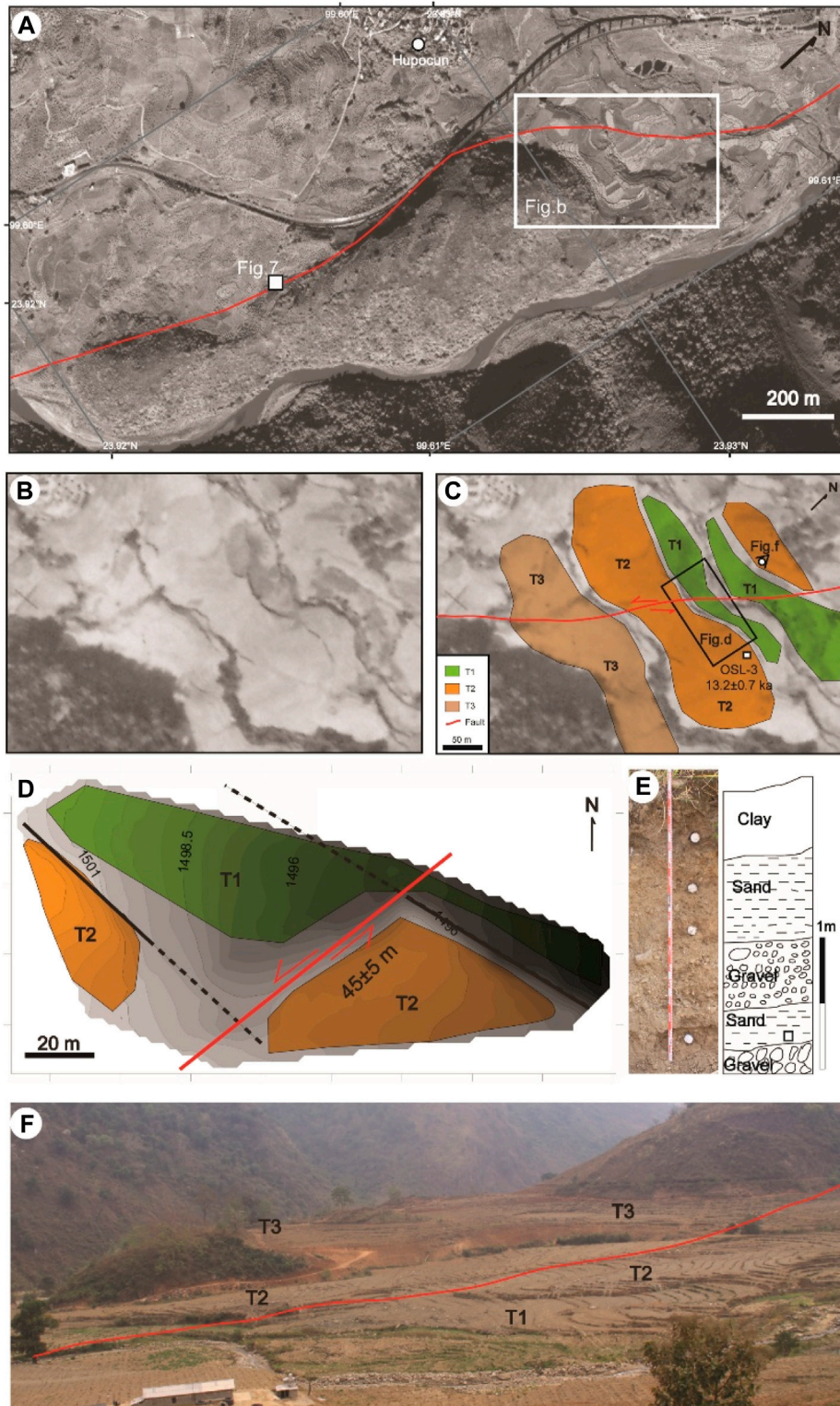


FIGURE 6 | Map of offset fill terraces at Hupocun. **(A)** Gaofen 2 satellite image of Daxueshan, the white rectangle indicates the location of panel **(B)**, white square shows the location. **(B)** Original aerial photograph. **(C)** Geomorphic interpretation of the aerial photograph. Light green, orange, and brown polygons represent T1, T2, and T3 surfaces, respectively. Black rectangle indicates the location of panel **(D)** White square shows the location of the OSL sample (OSL-3) and its age (13.2 ± 0.7 ka). **(D)**, Topographic map of offset T1/T2 riser (0.5 m contour interval), obtained from differential GPS measuring system. **(E)** Photograph and log of the sampling profile. White square is the location of the OSL sample. **(F)** Photograph of terraces, viewing to the south.

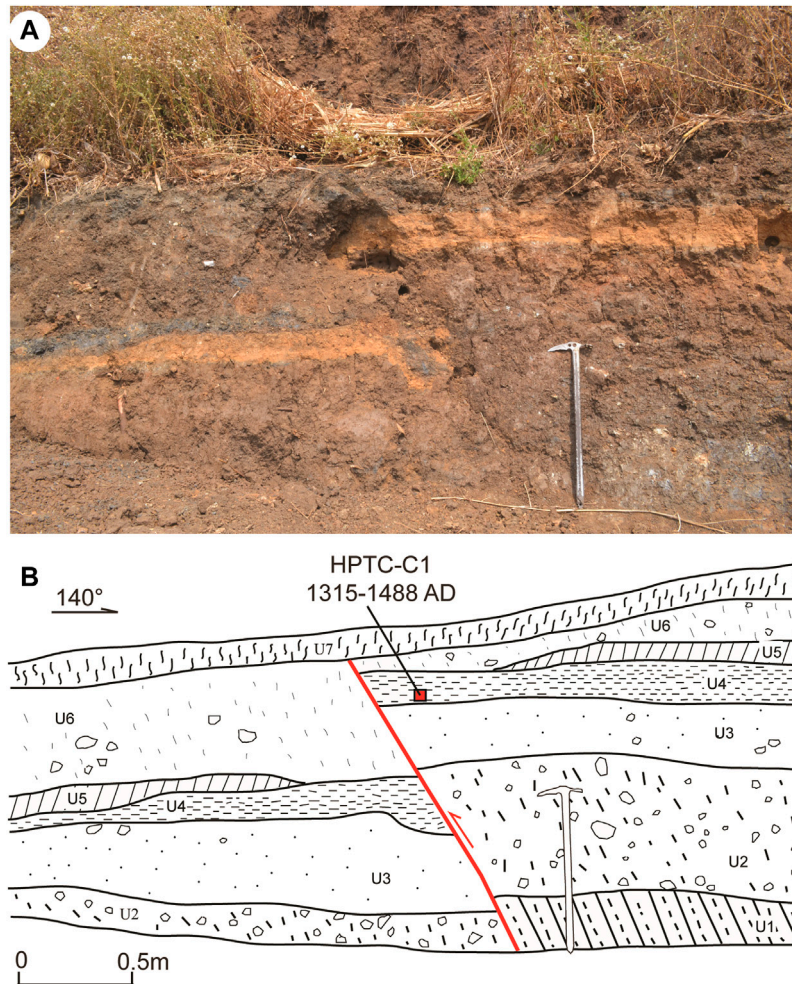


FIGURE 7 | Trench site on the Nantinghe fault at Hupocun. **(A)** Photo of the Hupo trench HPTC. **(B)** Log of the Hupo trench HPTC. Red square shows the location of the ^{14}C sample HPTC-C1. Ice ax for scale.

TABLE 3 | Lithologic units in the HPTC trench.

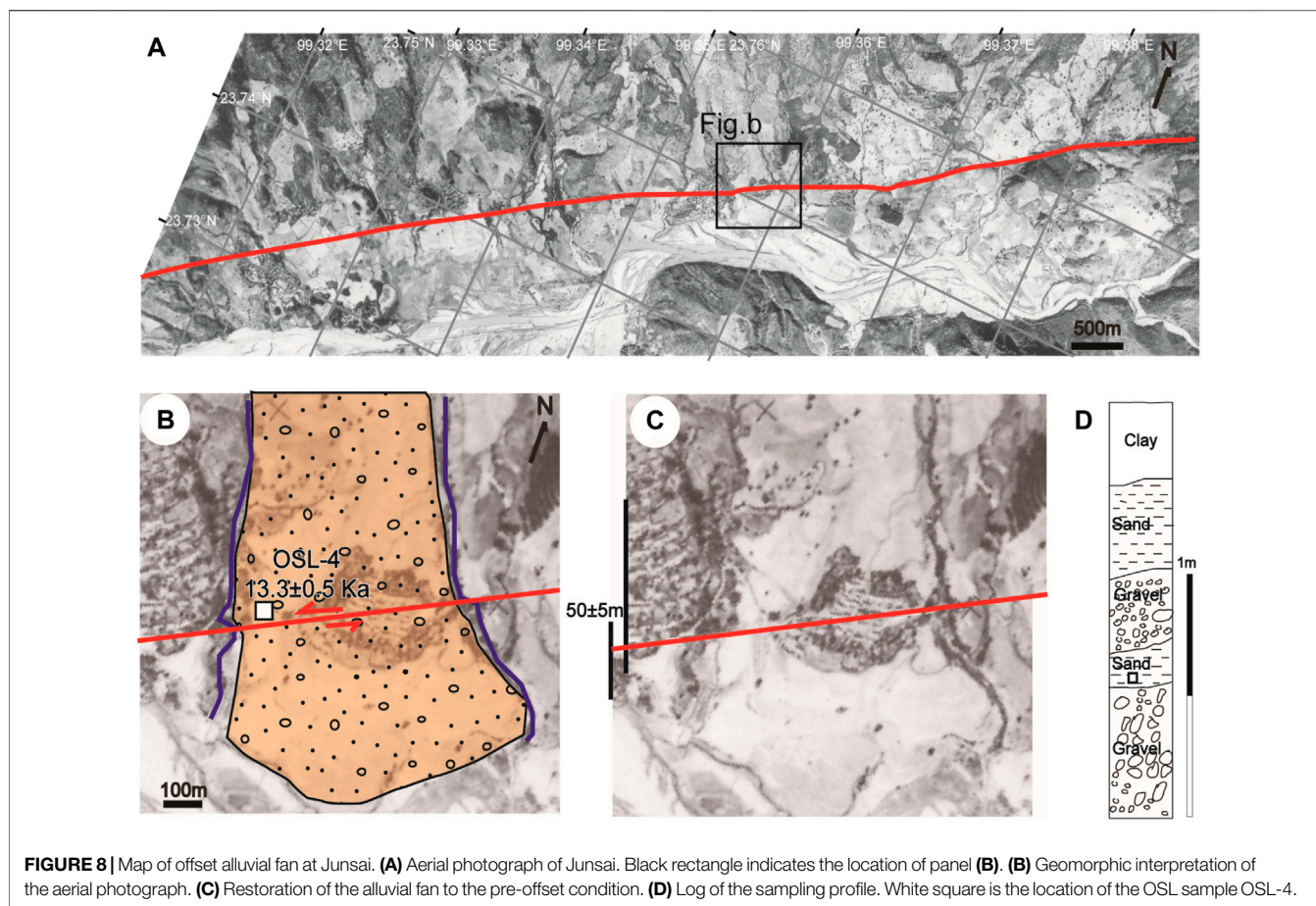
Unit	Description
U1	Devonian phyllite, weathered serious
U2	Grey gravel layer. The mean clast diameter is about 5 cm, with rare clasts over 10 cm
U3	Grey sand layer with rare small gravel
U4	Yellow clay layer with rare gravel
U5	Celadon sand layer with rare small gravel
U6	Grey gravel layer. The mean clast diameter is about 5 cm, with rare clasts over 10 cm
U7	plough layer

4.3 Hupocun

Three terraces (T1-T3) are found near Hupocun village, about 6 km southwest of the Daxueshan site (Figure 2). All terraces are cut by the Nantinghe fault (Figure 6). T3 is only preserved on the southern side of a creek. The throw is 10 m on the T3 terrace and 3–4 m on the T2 terrace and the T2/T1 riser is offset left-laterally

by about 50 m. We use the sinistral offsets of the T2/T1 riser and the T2 age to calculate the sinistral-slip rate, and the throw rate is estimated from the height of the scarp on T2 and the T2 age. The sinistral and vertical offsets, as obtained from DGPS surveys, are 45 ± 5 m and 4 ± 0.5 m, respectively. The age of T2 at this site is estimated at 13.2 ± 0.7 ka based on OSL dating on sample OSL-3 (Table 1). Thereby, the sinistral-slip rate and throw rate are 3.4 ± 0.6 mm/a and 0.3 ± 0.1 mm/a, respectively. Again, these rates are conservative estimates.

We also excavated a trench (HPTC) at this site, on the south of the terraces. The fill terraces at this site are typically composed of subhorizontal, crudely- to well-bedded gravel layers with a few sand layers. The HPTC trench was excavated in the alluvial fan with well-bedded sand layers. Seven distinct lithologic units were identified in the trench walls (Figure 7) and are described in Table 3. Only one fault plane was recognized. The fault cuts the units U1 to U6 and is overlain by U7, a plough layer (Figure 7). We collected a charcoal sample, HPTC-C1, from U4 (Figure 6) and obtained its ^{14}C age, 1315–1488 AD (Table 2).



4.4 Junsai

Further southwest, about 100 km from Yunxian County, we identified obvious offsets of the alluvial fan and the gully at a site near Junsai township (**Figure 8**). We measured horizontal offsets on the aerial photographs. The alluvial fan is sinistrally offset by about 50 m. OSL dating on sample OSL-4 yields 13.3 ± 0.5 ka for the age of the alluvial fan at this site (**Table 1**). Therefore, the sinistral-slip rate, at its minimum, is 3.8 ± 0.2 mm/a using the age and the displacement of the alluvial fan. Because of the artificial reforming, we could not obtain the vertical offset of the alluvial fan.

4.5 Mengjian

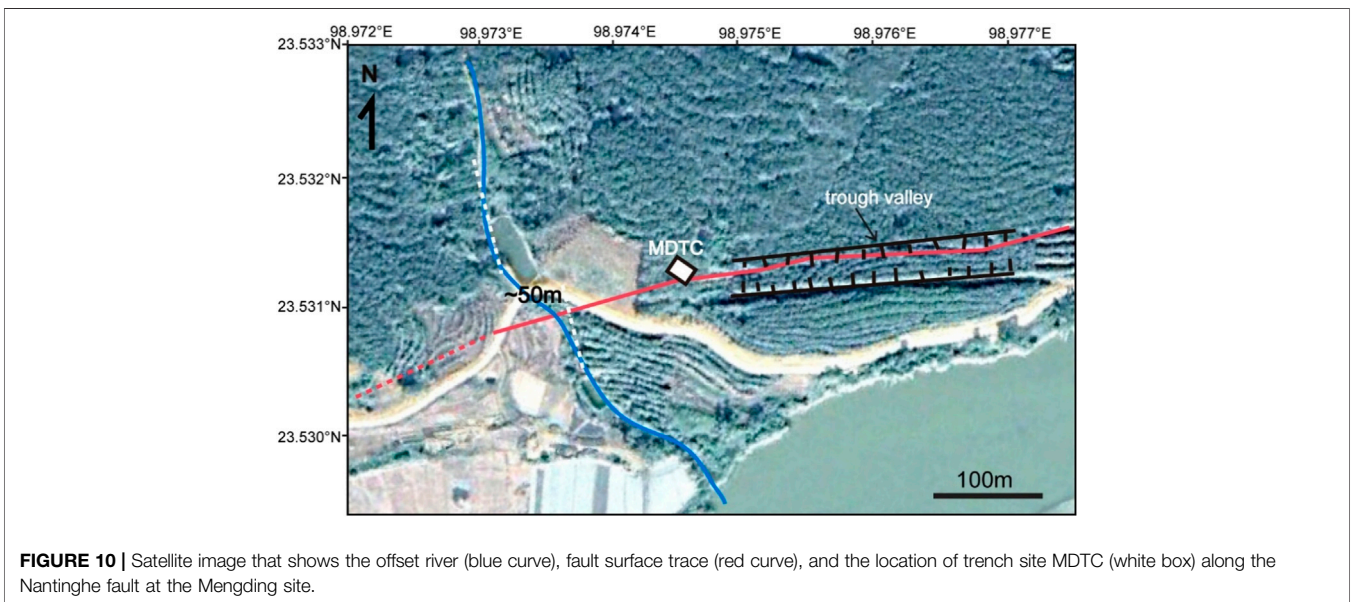
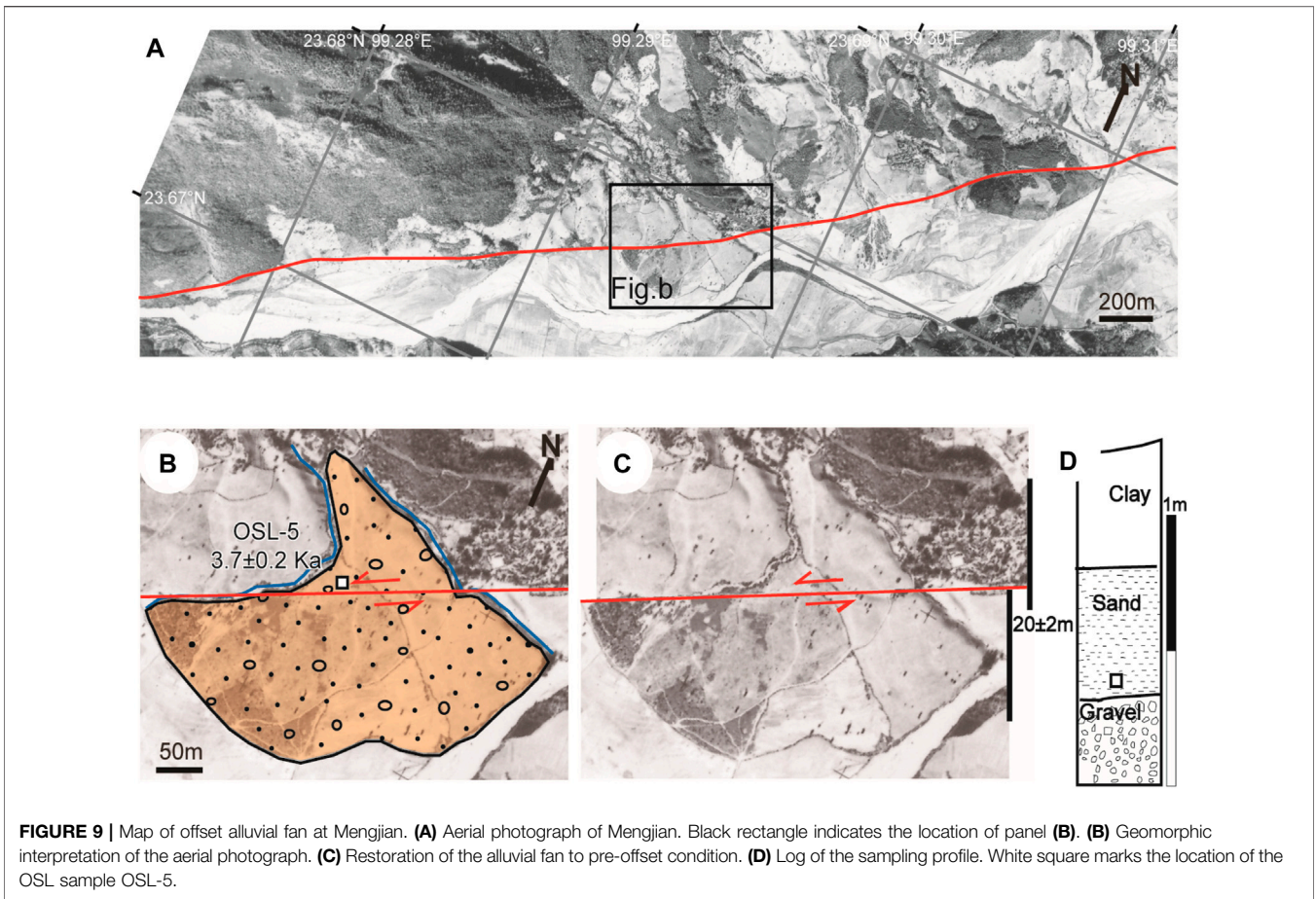
In the same Quaternary basin, west of Mengjian, offsets of an alluvial fan and a gully are clearly shown on the aerial photographs (**Figure 9**). We measured horizontal offsets from aerial photographs. The alluvial fan is left-laterally offset by about 20 m. The age of the alluvial fan at this site is 3.7 ± 0.2 ka based on OSL dating on sample OSL-5 (**Table 1**). Hence, the sinistral-slip rate is 5.4 ± 0.3 mm/a using the age and the sinistral offset of the alluvial fan. Due to artificial reforming, the vertical offset of the alluvial fan is too inexplicit to obtain.

4.6 Mengding

The Mending basin is the largest and deepest Quaternary basin along the Nantinghe fault (**Figure 2**). At the southeast

corner of the Mending basin, a river clearly shows left-laterally offset, marking the fault traces (**Figure 10**). We excavated a trench, MDTC, in the alluvial fan near the river, across to the fault trace (**Figure 11**). Exposed faults on the trench wall have high apparent dips ($>60^\circ$) to the northwest and show a top-NW normal sense of slip. Rocks in the footwall block of the master fault are composed primarily of consolidated gravel layer Unit 1, overlain by Unit 16 (**Table 4**). The presence of a resistant consolidated gravel layer at the footwall has allowed the accumulation of at least two distinct sediment wedges in the hanging wall. The fault system is expressed as a negative flower structure with a general dip to the north, and five separate fault planes can be identified.

The MDTC trench shows a prolific record of fault activity. Fault F1 cuts unit U1-U14 and appears to terminate at the base of U16. Fault F2 cuts U2-U11 and appears to terminate at the base of U12. Fault F3 truncates unit U2-U12 and is overlain by U14. Fault F4 offsets unit U2-U9 and is covered by U10. Fault F5 cuts U2-U13 and is concealed by U14. We infer that five paleoearthquake events are recorded by the faulting shown in this trench, all of which postdated the deposition of U2. Three ^{14}C samples, MDTC-C5, C17, and C38 were collected from U2, U5, and U11 layers, respectively, and their ages are 4970 ± 40 BP, 1710 ± 30 BP, and 690 ± 30 BP, respectively. An OSL sample, OSL-6, from U9 yields 1.1 ± 0.1 ka (**Tables 1, 2**).



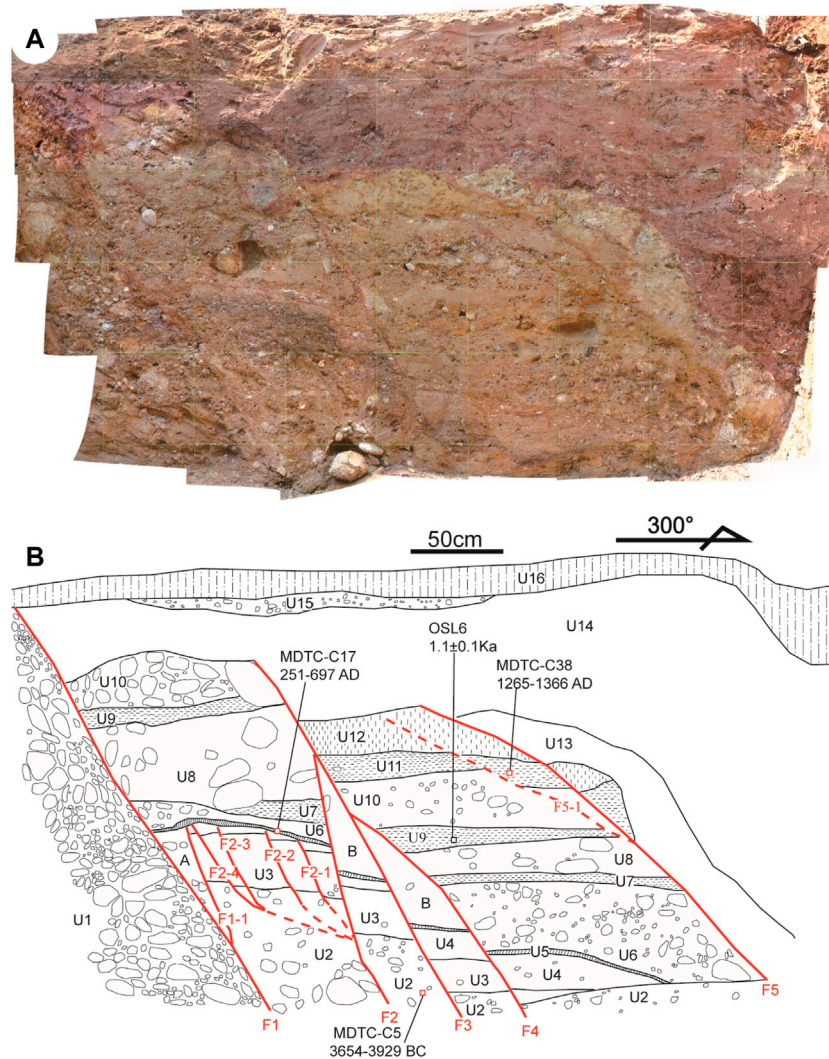


FIGURE 11 | Trench site on the Nantinghe fault at the Mengding site. **(A)** Photo of the Mengding trench (MDTC). **(B)** Log of the Mengding trench MDTC. Red line denotes fault. Sample locations for radiocarbon and OSL dating (MDTC-C5, C17, and C38, and OSL-6, respectively) and their ages are also annotated.

5 DISCUSSION

5.1 Paleoseismicity Records

Previous work revealed a ~45,000 year-long, incomplete paleoseismicity history in the northern segment of the Nantinghe fault (Sun et al., 2017). No earthquake greater than 6 along the Nantinghe fault is recorded in history so far, except for the 1941 M7 earthquake near the Myanmar-China border. In contrast, many earthquakes have occurred in the nearby region (Figure 1).

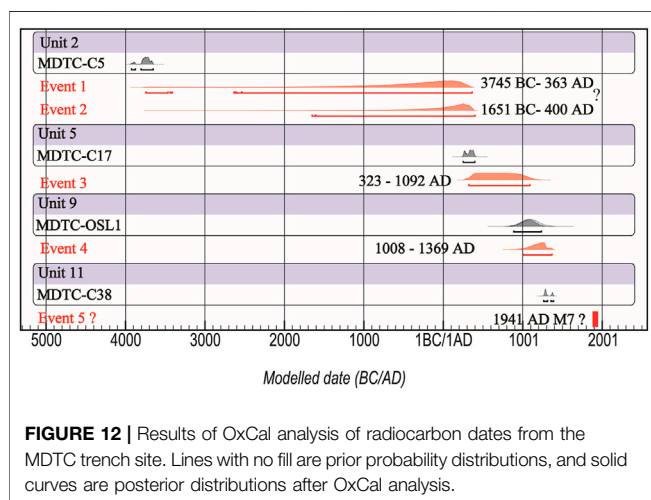
The Mengding trench MDTC provides us an opportunity to document the paleoseismicity. We use OxCal 4.3 with the three ^{14}C (MDTC-C5, MDTC-C17, MDTC-C38) samples and the OSL sample (OSL-6) to estimate the timing of the paleoseismicity events (Figure 12). At least four events are identified: event 1 (3745 BC–363 AD), event 2 (1651 BC–400 AD), event 3 (323–1092 AD),

and event 4 (1008–1369 AD), while the fifth event that corresponds to the 1941 AD M7 event is not revealed by our data.

We illustrate the sequence of these events in a set of diagrams (Figure 13). The first paleoseismicity event took place after the deposition of U2 and formed U3, which may be a sedimentary wedge (Figures 13A,B). Materials in U3 appear to be derived from U1. The ^{14}C sample MDTC-C5 from U2 indicates that the lower limit time of the first paleoseismicity event is 3929–3654 BC (Figure 12). Unit U4 was deposited after the first event (Figure 13C). The second paleoseismicity event occurred after the deposition of U4 and involved both faults F1 and F2 (Figure 13D). Unit U5 was deposited after the second event (Figure 13E). The third paleoseismicity event took place after the deposition of unit U5 and involved faults F1 and F2 (Figure 13F). The ^{14}C sample MDTC-C17 from U5 indicates that the upper limit time of the second paleoseismicity event and the

TABLE 4 | Lithologic units in the Mengding trench MDTC.

Unit	Description
U1	Grey-yellow coarse gravel layer, dominated by gravel and cobbles with a diameter of 3–5 cm and 15–20 cm, with rare clasts over 20 cm. The gravel is poorly sorted, the 3–5 cm gravel is poorly rounded but the 15–20 cm gravel is slightly rounded
U2	Grey gravel layer. The mean clast diameter is about 5 cm, with rare clasts over 10 cm
U3	Black sand gravel layer. Rich in organic matter and thins out from east to west
U4	Grey sand layer, thin out from east to west
U5	Prunusos clay with rare small gravel
U6	Grey gravel layer. The mean clast diameter is about 5 cm, with rare clasts over 10 cm
U7	Grey sand layer with rare small gravel
U8	Grey-yellow sand gravel layer
U9	Grey sand layer
U10	Grey gravel layer. The gravel is poorly sorted and is slightly rounded
U11	Grey sand layer
U12	Grey fine sand layer
U13	Grey-white sand clay layer
U14	Crimson clay layer with rare grey gravel. The top boundary is nearly horizontal, but the bottom boundary fluctuates and is affected by fault activity
U15	Tawny sandy gravel layer, dominated by gravel and cobbles with a diameter less than 2 cm. The gravel is generally sorted and finely rounded
U16	Artificial accumulation
A	Grey sand and fine gravel wedge. The grain size of the fine gravel is 3–5 cm. Materials in the wedge are similar to those mixtures that form U2, U3, and U4
B	Grey-yellow sand gravel wedge. Materials in the wedge are similar to those that form U8

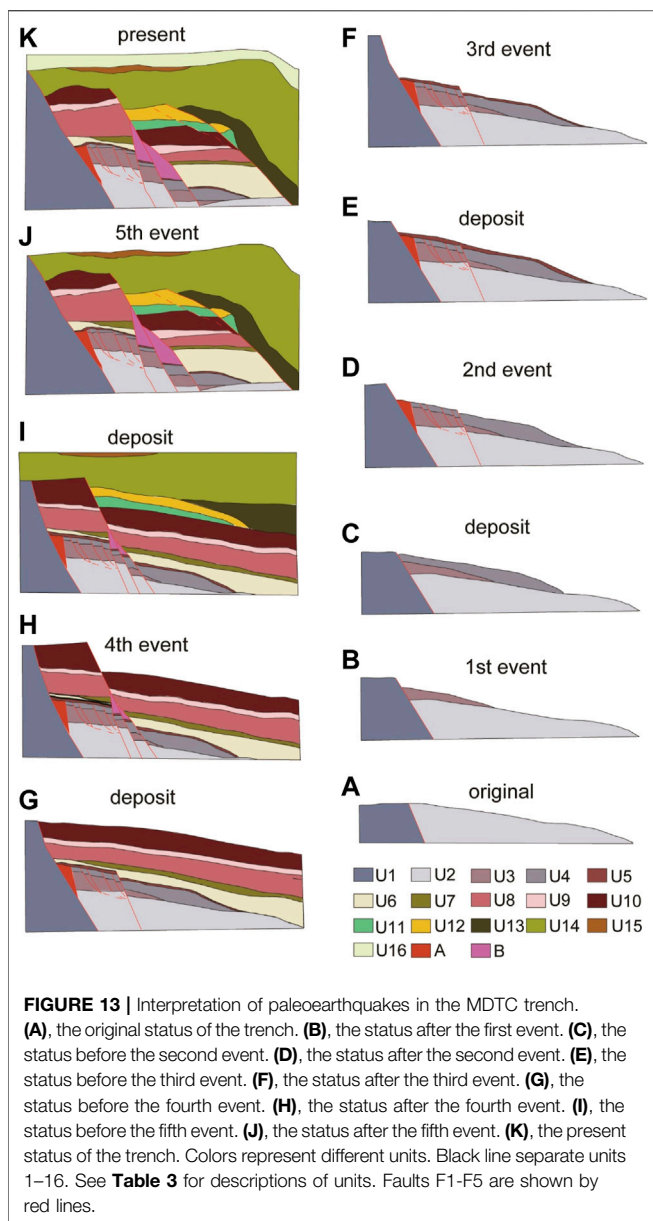


lower limit time of the third paleoearthquake were around 251–697 AD. Unit U6, U7, U8, U9, and U10 were deposited after the third event, which is compatible with the OLS age (ca. 1.1 ± 0.1 ka) from U9 (**Figure 13G**). The fourth paleoearthquake event happened after the deposition of unit U10 and involved faults F1, F2, F3, and F4 (**Figure 12H**). Unit U11, U12, U13, U14, and U15 were deposited after the fourth event (**Figure 12I**). Samples from U9 (OSL) and U11 (radiocarbon) bracket the time of the fourth paleoearthquake between 1.1 ka and 1265–1366 AD. The fifth paleoearthquake event took place after the deposition of U15 and involved faults F1, F2, F3, F4, and F5 (**Figure 13J**). Unit U16 was deposited after the fifth event. Due to the lack of well-documented history in this region prior to the Ming and Qing Dynasties (1368–1911 AD), no destructive paleoearthquake in the Historical Strong Earthquake Catalog of China (China

Earthquake Administration, 1995) can be associated. Thus, the fifth event may be related to the 1941 M7 historical earthquake.

For the Hupocun trench HPTC, based on the age of U4 there (^{14}C age 520 ± 40 B.P.) (**Figure 6; Table 2**) and the only record of the strong earthquake (1941 M7) in this areas, we attribute the youngest deformation also to the 1941 M7 event.

Our results also place important constraints on the occurrence times of paleoearthquake events on the Nantinghe fault. One paleoearthquake event is recorded in the trench at Hupocun (**Figure 7**). The event occurred after 1315–1448 AD. Based on our work on the Mengding trench, there are five paleoearthquake events in the last 5,000 a, and four paleoearthquake events between 3929 BC and 1366 AD. Since the distance between Hupocun and Mengding is only 60 km and there is no obvious step or discontinuity in the fault trace over this distance, we suggest that the faults in Hupocun and Mengding are likely to have similar rupture histories. If this is true, then we can analyze earthquake occurrence times using paleoearthquakes from the two trench sites and historical earthquakes. One documented historical earthquake occurred in AD 1941. Thus, the youngest events in the MDTC trench may be equivalent to that in the HPTC trench, which postdated 1315–1448 AD. Since the faults almost ruptured the surface in both trenches, we speculate that the youngest event in the two trenches corresponds to the 1941 M7 event. Five paleoearthquakes occurred during the last 5,000 years (yielding an approximate recurrence interval of $\sim 1,000$ a). Given slip rates of 3.5–5.4 mm/a, the millennial displacement should be 3.5–5.4 m. The magnitude of the earthquake generated by the latest event is an important parameter in evaluating earthquake hazards in a region. It depends on the coseismic rupture length, displacement, and history records. Associate with the history records, the last earthquake along the Nantinghe fault was estimated to be an M7 event (China Earthquake



Administration, 1995). According to the empirical relationships between the magnitude, surface rupture length, and displacement on strike-slip faults around the Tibetan Plateau (Deng et al., 1992; Ye et al., 1996), a surface rupture length of 60 km and a maximum displacement of 3.5–5.4 m suggest a magnitude ranging from Ms 7.4 to 7.6. Additionally, the empirical relationship of (Wells and Coppersmith, 1994) points to Ms 7.2–7.7. Moreover, the 1988 Ms 7.6 and 7.2 Lancang-Gengma earthquakes in the nearby region produced two surface ruptures of ~50 and ~14 km, respectively (Yu et al., 1991). Therefore, the magnitude of the latest earthquake is likely to be in the range of Ms 7.0–7.7.

5.2 Slip Rate Estimate

The methodologies for estimating slip rates are often debated due to the various proxies and time scales. For the large strike-slip faults

within the Indo-Asian collision zone and other regions around the world (Van Der Woerd et al., 2002; Tong et al., 2014), geodetically-determined slip rates are generally different from those reported using reconstructions of offset landforms, and it is unclear if this discrepancy reflects true secular variation in slip history, systematic errors in interpretation, or both. Even slip rates derived from different reconstructions of offset landforms along the same fault can be different. A major potential source of uncertainty when assessing slip rates from offset fill terraces is the underlying geomorphic model of terrace formation and abandonment that must be assumed (Mériaux et al., 2004; Cowgill, 2007). One evolutionary model suggests that the erosion of the flood plain and its banks continues until the river begins to incise and new terraces form (Van Der Woerd et al., 2002). According to this model, the offset of a terrace riser only begins to accumulate once the lower terrace is abandoned. An alternative model allows for differences in erosion patterns between the sides of the river, in which case riser offsets may begin to accumulate after the upper terrace is abandoned. For example, at a site on the Altyn Tagh fault, a study used the offset of a terrace riser and the abandonment age of the lower terrace to obtain a slip rate of 25.9 ± 1.8 mm/a (Mériaux et al., 2004). Using the abandonment age of the higher terrace, a competing study yielded a slip rate of 9–10 mm/a (Cowgill, 2007). Thus, the choice of a conceptual model is the key to slip rate evaluation but remains controversial. Using the alluvial fan to calculate the slip rate, however, can avoid this issue.

At the Zhujiacun, Daxueshan, and Hupocun sites, we used the ages of the higher terraces to determine the slip rate of the Nantinghe fault. At the Junsai and Mengjian sites, slip rates are calculated from the offset alluvial fan. The slip rates from the two approaches agree with each other (between 3.5 and 5.4 mm/a), indicating that the higher terrace approach is more suitable.

We calculated the mean slip rate using the maximum likelihood regression *via* IsoplotR (Vermeesch, 2018) based on the modified error-weighted least-squares algorithm of York et al. (2004) (Figure 14A). Due to the lack of slip rates, previous studies have debated whether different segments of the Nantinghe fault have different activities. From the depth of the basin, which decreases northeastward along the fault, and the occurrence of the 1941 M7 earthquake, it seemed that the northeastern segment may be less active than the southwestern segment (Zhu et al., 1994; Wang et al., 2006) (Figure 2). Nevertheless, our results of 4.0 ± 0.6 (2σ) mm/a reveal a similar Quaternary activity along the Nantinghe fault (Figures 2, 14A).

5.3 Tectonic Implications

Our results provide clear evidence for the late Quaternary oblique sinistral-thrust activity on the Nantinghe fault; its millennial strike-slip rate is ca. 3.9 ± 0.6 (2σ) mm/a, in agreement with the GPS measurements (4 mm/a) (Wang, 2009). The Nantinghe fault also shows a 0.3–0.6 mm/a slip rate in the dip-slip orientation. These slip rates help us constrain the applicability of the competing tectonic models for the Tibetan Plateau. The block models require large strike-

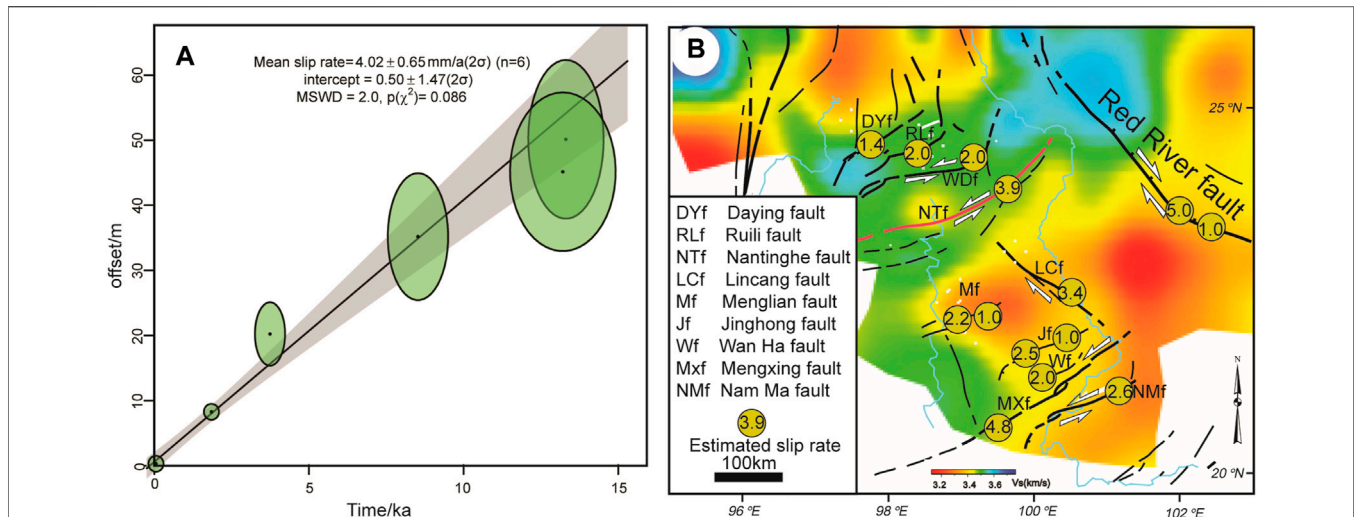


FIGURE 14 | (A) Mean left-lateral slip rate of the Nantinghe fault. The maximum likelihood regression is calculated via IsoplotR (Vermeesch, 2018) based on the modified error-weighted least-squares algorithm of York et al. (2004). **(B)** Integrated map of estimated slip rates (mm/yr) in the study area. Base map is the shear-wave velocity model at 21 km from (Bao et al., 2015). Sources for slip rates on the faults, from north to south, include: Daying fault (Chang et al., 2011); Ruili fault (Huang et al., 2010; Wang et al., 2014); Wanding fault (Chang et al., 2012); Nantinghe fault, this study; Lincang fault (Wang et al., 2014); Mengliang fault (Wang et al., 2014; Liu et al., 2019); Jinghong fault (Shi et al., 2018c); Wan Ha fault (Wang et al., 2014); Mengxing fault (Lacassin et al., 1998; Wang et al., 2014); Nam Ma fault (Lacassin et al., 1998; Wang et al., 2014); and Red River fault (Replumaz et al., 2001; Shi et al., 2018a).

TABLE 5 | Summary of Quaternary slip rates along the major faults in Southeastern Tibetan Plateau.

Fault name	Sense-of-motion	Strike-slip rate (mm/a)	Dating method ^a	References
Daying	sinistral	1.4	TL	Chang et al. (2011)
Ruili	sinistral	2.0	OSL/TL	Huang et al. (2010)
Wanding	sinistral	2.0	TL	Chang et al. (2012)
Nantinghe	sinistral	4.0	OSL/ ¹⁴ C	This study
Lincang	dextral	3.4	estimation	Wang et al. (2014)
Mengliang	sinistral	2.2	OSL	Liu et al. (2019)
Jinghong	sinistral	1.0	estimation	Wang et al. (2014)
		2.5	¹⁴ C	Shi et al. (2018c)
		1.0	estimation	Wang et al. (2014)
Wan Ha	sinistral	2.0	estimation	Wang et al. (2014)
Mengxing	sinistral	4.8	estimation	Lacassin et al. (1998), Wang et al. (2014)
Nam Ma	sinistral	2.6	estimation	Lacassin et al. (1998), Wang et al. (2014)
Red River	dextral	5.0	Estimation	Replumaz et al. (2001)
		1.0	¹⁴ C	Shi et al. (2018a)

^aTL, thermoluminescence; OSL, optically stimulated luminescence.

slip rates at the boundaries between different tectonic blocks, but small strike-slip rates within tectonic blocks (Leloup et al., 1995; Tapponnier et al., 2001). On the contrary, the continuum models (England and Molnar, 2005; Copley, 2008) do not necessarily predict such large slip rates at boundaries between different tectonic blocks, but larger strike-slip rates within tectonic blocks.

Moderate to high Quaternary slip rates have been found on the major strike-slip faults within the Indochina Block, including the Daying, Ruili, Wangding, Nantinghe, Lincang, Jinghong, Wan Ha, Mengxing, and Nan Ma faults (Table 5). Their strike-slip rates range from 1.0 to 5.0 mm/a. By contrast, the Red River fault, albeit a plate boundary fault in geologic history, shows a comparable dextral-slip

rate of up to 1–5 mm/a over decadal, millennial, and million-year timescales (Allen et al., 1984; Weldon et al., 1994; Copley, 2008; Shi et al., 2018a; Replumaz et al., 2001; Schoenbohm et al., 2006) (Figure 13B). Moreover, as pointed out by Shi et al. (2018b), the distinct arcuate geometry of the sinistral strike-slip faults and the curved GPS velocity field are difficult to reconcile with the block models but can be readily explained in the continuum models.

An asymmetric, tongue-shaped GPS velocity pattern is found across the Indochina Block from Sunda to the Eastern Himalayan Syntaxis (Shi et al., 2018b). In turn, Shi et al. (2018b) proposed that asthenospheric flow exerts basal traction to the overlying lithosphere and induces the faulting in the upper crust. The Nantinghe fault, with its 3.5–5.4 mm/a millennial slip rate, is

located in a swath of the largest slip rate on the velocity profile by Shi et al. (2018b). Interestingly, this swath, containing the Daying, Ruili, Wanding, and Nantinghe faults on the surface, is located between two localized, NE-SW-trending channels of low-velocity anomalies at the mid-crustal depths from a high-resolution shear-wave seismic tomography model of this region (Bao et al., 2015), (Figure 13B). All these results indicate that the Red River fault does not dominate the present-day kinematics of the Indochina Block, and hence the continuum models could play a more dominant role in the Quaternary tectonics of this region. Pre-existing crustal weakness (such as the Red River and Nantinghe faults) and crustal heterogeneities promote the lateral variations in the lower crustal strength, which shaped the upper-crustal deformation and topography (Tan et al., 2019; Penney and Copley, 2021).

6 CONCLUSION

We have documented the Quaternary activity of the Nantinghe fault in the Southeastern Tibetan Plateau region, using a combination of field observation, satellite and aerial imagery interpretation, trenching, and ^{14}C and OSL geochronology. The Nantinghe fault has been active in the latest Quaternary with an oblique sinistral-thrust sense of slip. Detailed geochronology and fault kinematic measurements on the sinistral displacement reveal that the sinistral strike-slip rates along the fault are ca. 4.0 ± 0.6 (2σ) mm/a over the past 13 ka. Apparent throw rates are typically less than 1 mm/a. Our trench investigations demonstrate at least four 4) Holocene earthquakes along the Nantinghe fault, suggesting an averaged recurrence interval of $\sim 1,000$ a. The newly-obtained slip rates on the Nantinghe fault, integrated with previous estimates on other faults in this region, provide direct evidence that favors the continuum models over the rigid block ones, which advances our knowledge on the deformation mechanism in the India-Asia continental collision.

REFERENCES

- Aitken, M. J. (1998). *An Introduction to Optical Dating: The Dating of Quaternary Sediments by the Use of Photon-Stimulated Luminescence*. Oxford, New York, Tokyo: Oxford University Press, 267.
- Allen, C. R., Gillespie, A. R., Yuan, H., Sieh, K. E., Buchun, Z., and Chengnan, Z. (1984). Red River and Associated Faults, Yunnan Province, China: Quaternary Geology, Slip Rates, and Seismic hazard. *Geol. Soc. America Bull.* 95, 686–700. doi:10.1130/0016-7606(1984)95<686:rraafy>2.0.co;2
- Avouac, J.-P., and Tapponnier, P. (1993). Kinematic Model of Active Deformation in central Asia. *Geophys. Res. Lett.* 20, 895–898. doi:10.1029/93gl00128
- Bao, X., Sun, X., Xu, M., Eaton, D. W., Song, X., Wang, L., et al. (2015). Two Crustal Low-Velocity Channels beneath SE Tibet Revealed by Joint Inversion of Rayleigh Wave Dispersion and Receiver Functions. *Earth Planet. Sci. Lett.* 415, 16–24. doi:10.1016/j.epsl.2015.01.020
- Bronk Ramsey, C. (2009). Bayesian Analysis of Radiocarbon Dates. *Radiocarbon* 51 (1), 337–360. doi:10.1017/s0033822200033865
- Chang, Z.-F., An, X., and Zhang, Y. (2012). Study on Late-Quaternary Activity and Displacement of Drainage Systems along the Wanding Fault (In Chinese with English Abstract). *Seismology Geology*. 34 (2), 228–239.

DATA AVAILABILITY STATEMENT

The original contributions presented in the study are included in the article/**Supplementary Material**, further inquiries can be directed to the corresponding author.

AUTHOR CONTRIBUTIONS

Conceptualization was performed by FS and HH, the fieldwork was done by FS, ZW, and HS, the writing and preparation of the original draft were conducted by FS, the review and editing of the final manuscript were performed by FS and YL. All authors have read and agreed to the published version of the manuscript.

FUNDING

This work was jointly supported by the National Key Research and Development Program of China (2021YFC3000601), the National Natural Science Foundation of China (41702221) and the China Active Fault Survey Project (201102001).

ACKNOWLEDGMENTS

We thank the two Reviewers Drs. Hu Wang and Bo Zhang for providing prompt and constructive reviews. YL acknowledges the Governor's University Research Initiative (GURI) fund from the State of Texas and the University of Houston.

SUPPLEMENTARY MATERIAL

The Supplementary Material for this article can be found online at: <https://www.frontiersin.org/articles/10.3389/feart.2021.818225/full#supplementary-material>

- Chang, Z.-F., Chen, G., and Yu, J.-Q. (2011). Geological Evidence of Activity along the Dayingjiang Fault since Late Pleistocene (In Chinese with English Abstract). *Seismology Geology*. 33 (4), 877–888.
- Chen, G., Xu, X., Wen, X., and WangZheng, Y. R. (2006). Application of Digital Aerophotogrammetry in Active Tectonics (In Chinese with English Abstract). *Earth Science-Journal China Univ. Geosciences* 31 (3), 405–410.
- China Earthquake Administration (1995). *Historical Strong Earthquake Catalog of China (2300 BC-1911 AD)*. Beijing: Earthquake Publishing House. (in Chinese).
- China Earthquake Administration (1999). *Recent Earthquake Catalog of China (1912-1990, Ms \geq 4.7)*. Beijing: Earthquake Publishing House. (in Chinese).
- China Earthquake Networks Center (2019). Seismological Data Service System. Available at: [Http://www.csndmc.ac.cn/newweb/data.html](http://www.csndmc.ac.cn/newweb/data.html).
- Copley, A. (2008). Kinematics and Dynamics of the southeastern Margin of the Tibetan Plateau. *Geophys. J. Int.* 174, 1081–1100. doi:10.1111/j.1365-246x.2008.03853.x
- Cowgill, E. (2007). Impact of Riser Reconstructions on Estimation of Secular Variation in Rates of Strike-Slip Faulting: Revisiting the Cherchen River Site along the Altyn Tagh Fault, NW China. *Earth Planet. Sci. Lett.* 254, 239–255. doi:10.1016/j.epsl.2006.09.015
- Deng, Q. D. (2007). *Map of Active Tectonics in China*. Beijing: Seismological Press.
- Deng, Q. D., Yu, G. H., and Ye, W. H. (1992). "Relationship between Earthquake Magnitude and Parameters of Surface Ruptures Associated with Historical

- Earthquakes (In Chinese with English Abstract),” in *Research on Active Fault* (2). Editor Q. D. Deng (Beijing, China: Seismological Press), 247–264.
- Dewey, J. F., Pitman, W. C., Ryan, W. B. F., and Bonnin, J. (1973). Plate Tectonics and the Evolution of the Alpine System. *Geol. Soc. America Bull.* 84, 3137–3180. doi:10.1130/0016-7606(1973)84<3137:ptateo>2.0.co;2
- Di Giacomo, D., Engdahl, E. R., and Storchak, D. A. (2018). The ISC-GEM Earthquake Catalogue (1904-2014): Status after the Extension Project. *Earth Syst. Sci. Data* 10, 1877–1899. doi:10.5194/essd-10-1877-2018
- England, P., and Houseman, G. (1986). Finite Strain Calculations of continental Deformation: 2. Comparison with the India-Asia Collision Zone. *J. Geophys. Res.* 91, 3664–3676. doi:10.1029/jb091ib03p03664
- England, P., and McKenzie, D. (1982). A Thin Viscous Sheet Model for continental Deformation. *Geophys. J. Int.* 70, 295–321. doi:10.1111/j.1365-246x.1982.tb04969.x
- England, P., and Molnar, P. (2005). Late Quaternary to Decadal Velocity fields in Asia. *J. Geophys. Res.* 110, B12401. doi:10.1029/2004jb003541
- He, H. L., Ikeda, Y., Song, F. M., and Dong, X. Q. (2002). Late Quaternary Slip Rate of the Xiaojiang Fault and its Implication (In Chinese with English Abstract). *Seismology Geology*. 24 (1), 14–26.
- He, H. L., and Oguchi, T. (2008). Late Quaternary Activity of the Zemuhe and Xiaojing Fault in the Southwest China from Geomorphological Mapping. *Geomorphology* 96 (1-2), 62–85. doi:10.1016/j.geomorph.2007.07.009
- Huang, J. Q., and Ren, J. S. (1987). *Geotectonic Evolution of China*. Berlin: Springer-Verlag.
- Huang, X.-M., Du, Y., Shu, S.-B., and Xie, F.-R. (2010). Study of the Late Quaternary Slip Rate along the Northern Segment on the South branch of Longling-Ruili Fault (In Chinese with English Abstract). *Seismology Geology*. 32 (2), 222–232.
- Kristen Clark, M., and Handy Royden, L. (2000). Topographic Ooze: Building the Eastern Margin of Tibet by Lower Crustal Flow. *Geology* 28 (8), 703–706. doi:10.1130/0091-7613(2000)028<0703:totbem>2.3.co;2
- Lacassin, R., Replumaz, A., and Hervé Leloup, P. (1998). Hairpin River Loops and Slip-Sense Inversion on Southeast Asian Strike-Slip Faults. *Geol* 26 (8), 703–706. doi:10.1130/0091-7613(1998)026<0703:hrlass>2.3.co;2
- Leloup, P. H., Lacassin, R., Tapponnier, P., Schärer, U., Zhong, D. L., LiuZhang, X. H. L. S., et al. (1995). The Ailao Shan-Red River Shear Zone (Yunnan, China), Tertiary Transform Boundary of Indochina. *Tectonophysics* 251 (1), 3–84. doi:10.1016/0040-1951(95)00070-4
- Leloup, P. H., Tapponnier, P., Lacassin, R., and Searle, M. P. (2007). Discussion on the Role of the Red River Shear Zone, Yunnan and Vietnam, in the continental Extrusion of SE Asia Journal, Vol. 163, 2006, 1025-1036. *J. Geol. Soc.* 164 (6), 1253–1260. doi:10.1144/0016-76492007-065
- Liu, B., Yuan, D., Wang, A., He, W., Shao, Y., Fang, L., et al. (2019). Accurate Determination of Late Quaternary Slip Rate of the Menglian Fault in Southwest Yunnan (In Chinese with English Abstract). *China Earthquake Eng. J.* 41 (3), 770–780.
- McCalpin, J. P. (1996). *Paleoseismology*. New York: Elsevier, 588.
- Meade, B. J. (2007). Present-day Kinematics at the India-Asia Collision Zone. *Geol* 35, 81–84. doi:10.1130/g22924a.1
- Mériaux, A. S., Ryerson, F. J., Tapponnier, P., van der Woerd, J., Finkel, R. C., Xu, X., et al. (2004). Rapid Slip along the central Altyn Tagh Fault: Morphochronologic Evidence from Cherchen He and SulamuTagh. *J. Geophys. Res. Solid Earth* 109, B06401.
- Molnar, P., and Tapponnier, P. (1975). Cenozoic Tectonics of Asia: Effects of a Continental Collision: Features of Recent continental Tectonics in Asia Can Be Interpreted as Results of the India-Eurasia Collision. *Science* 189, 419–426. doi:10.1126/science.189.4201.419
- Peltzer, G., and Saucier, F. (1996). Present-day Kinematics of Asia Derived from Geological Fault Rates. *J. Geophys. Res. Solid Earth* 101 (B12), 27943–27956. doi:10.1029/96jb02698
- Penney, C., and Copley, A. (2021). Lateral Variations in Lower Crustal Strength Control the Temporal Evolution of Mountain Ranges: Examples from South-East Tibet. *Geochem. Geophys. Geosyst.* 22, e2020GC009092. doi:10.1029/2020GC009092
- Replumaz, A., Lacassin, R., Tapponnier, P., and Leloup, P. H. (2001). Large River Offsets and Plio-Quaternary Dextral Slip Rate on the Red River Fault (Yunnan, China). *J. Geophys. Res.* 106 (B1), 819–836. doi:10.1029/2000jb900135
- Royden, L. H., Burchfiel, B. C., and van der Hilst, R. D. (2008). The Geological Evolution of the Tibetan Plateau. *Science* 321, 1054–1058. doi:10.1126/science.1155371
- Schoenbohm, L. M., Burchfiel, B. C., Liangzhong, C., and Jiyun, Y. (2006). Miocene to Present Activity along the Red River Fault, China, in the Context of continental Extrusion, Upper-Crustal Rotation, and Lower-Crustal Flow. *Geol. Soc. America Bull.* 118 (5–6), 672–688. doi:10.1130/b25816.1
- Shen, Z. K., Lü, J. N., Wang, M., and Bürgmann, R. (2005). Contemporary Crustal Deformation Around the Southeast Borderland of the Tibetan Plateau. *J. Geophys. Res. Solid Earth* 110 (B11), B11409. doi:10.1029/2004jb003421
- Shi, F., He, H., Densmore, A. L., Li, A., Yang, X., and Xu, X. (2016). Active Tectonics of the Ganzi-Yushu Fault in the southeastern Tibetan Plateau. *Tectonophysics* 676, 112–124. doi:10.1016/j.tecto.2016.03.036
- Shi, F. (2014). *Tectonic Geomorphology of the Nantinghe Fault in Southwestern Yunnan*. Beijing: China Earthquake Administration. Institute of Geology (in Chinese with English abstract), PhD Dissertation.
- Shi, X., Sieh, K., Weldon, R., Zhu, C., Han, Y., Yang, J., et al. (2018). Slip Rate and Rare Large Prehistoric Earthquakes of the Red River Fault, Southwestern China. *Geochem. Geophys. Geosyst.* 19, 2014–2031. doi:10.1029/2017gc007420
- Shi, X., Wang, Y., Sieh, K., Weldon, R., Feng, L., Chan, C.-H., et al. (2018). Fault Slip and GPS Velocities across the Shan Plateau Define a Curved Southwestward Crustal Motion Around the Eastern Himalayan Syntaxis. *J. Geophys. Res. Solid Earth* 123 (3), 2502–2518. doi:10.1002/2017jb015206
- Shi, X., Weldon, R., Liu-Zeng, J., Wang, Y., Weldon, E., Sieh, K., et al. (2018). Limit on Slip Rate and Timing of Recent Seismic Ground-Ruptures on the Jinghong Fault, SE of the Eastern Himalayan Syntaxis. *Tectonophysics* 734–735, 148–166. doi:10.1016/j.tecto.2018.04.011
- Storchak, D. A., Di Giacomo, D., Bondar, I., Engdahl, E. R., Harris, J., Lee, W. H. K., et al. (2013). Public Release of the ISC-GEM Global Instrumental Earthquake Catalogue (1900-2009). *Seismological Res. Lett.* 84 (5), 810–815. doi:10.1785/0220130034
- Storchak, D. A., Di Giacomo, D., Engdahl, E. R., Harris, J., Bondar, I., Lee, W. H. K., et al. (2015). The ISC-GEM Global Instrumental Earthquake Catalogue (1900-2009): Introduction. *Phys. Earth Planet. Interiors* 239, 48–63. doi:10.1016/j.pepi.2014.06.009
- Sun, H., He, H., Wei, Z., Shi, F., and Gao, W. (2017). Late Quaternary Paleoseismicity along the Northern Segment of the Nantinghe Fault on the southeastern Margin of the Tibetan Plateau. *J. Asian Earth Sci.* 138, 258–271. doi:10.1016/j.jseae.2017.02.023
- Tan, X., Liu, Y., Lee, Y.-H., Lu, R., Xu, X., Suppe, J., et al. (2019). Parallelism between the Maximum Exhumation belt and the Moho Ramp along the Eastern Tibetan Plateau Margin: Coincidence or Consequence? *Earth Planet. Sci. Lett.* 507, 73–84. doi:10.1016/j.epsl.2018.12.001
- Tapponnier, P., Lacassin, R., Leloup, P. H., Schärer, U., Dalai, Z., Haiwei, W., et al. (1990). The Ailao Shan/Red River Metamorphic belt: Tertiary Left-Lateral Shear between Indochina and South China. *Nature* 343 (6257), 431–437. doi:10.1038/343431a0
- Tapponnier, P., Zhiqin, X., Roger, F., Meyer, B., Arnaud, N., Wittlinger, G., et al. (2001). Oblique Stepwise Rise and Growth of the Tibet Plateau. *Science* 294, 1671–1677. doi:10.1126/science.105978
- Taylor, M., and Yin, A. (2009). Active Structures of the Himalayan-Tibetan Orogen and Their Relationships to Earthquake Distribution, Contemporary Strain Field, and Cenozoic Volcanism. *Geosphere* 5 (3), 199–214. doi:10.1130/ges00217.1
- Thatcher, W. (2007). Microplate Model for the Present-Day Deformation of Tibet. *J. Geophys. Res.* 112, B01401. doi:10.1029/2005JB004244
- Tong, X., Smith-Konter, B., and Sandwell, D. T. (2014). Is There a Discrepancy between Geological and Geodetic Slip Rates along the San Andreas Fault System? *J. Geophys. Res. Solid Earth* 119 (3), 2518–2538. doi:10.1002/2013jb010765
- Van Der Woerd, J., Tapponnier, P., Ryerson, F. J., Mériaux, A.-S., Meyer, B., Gaudemer, Y., et al. (2002). Uniform Postglacial Slip-Rate along the central 600 Km of the Kunlun Fault (Tibet), from ²⁶Al, ¹⁰Be, and ¹⁴C Dating of Riser Offsets, and Climatic Origin of the Regional Morphology. *Geophys. J. Int.* 148, 356–388. doi:10.1046/j.1365-246x.2002.01556.x
- Vermeesch, P. (2018). IsoplotR: A Free and Open Toolbox for Geochronology. *Geosci. Front.* 9 (5), 1479–1493. doi:10.1016/j.gsf.2018.04.001

- Wang, E., Burchfiel, B. C., Royden, L. H., Chen, L., Chen, J., Li, W., et al. (1998). Late Cenozoic Xianshuihe-Xiaojiang, Red River, and Dali Fault Systems of Southwestern Sichuan and central Yunnan, China. *Geol. Soc. America Spec. Pap.* 327, 1–108. doi:10.1130/0-8137-2327-2.1
- Wang, J. N., Wang, Y. L., An, X. W., and Yang, X. D. (2006). Analysis of Latest Activity on NE-segment of west branch of Nantinghe Fault (In Chinese with English Abstract). *J. Seismological Res.* 29 (3), 264–268.
- Wang, Y., Sieh, K., Tun, S. T., Lai, K. Y., and Myint, T. (2014). Active Tectonics and Earthquake Potential of the Myanmar Region. *J. Geophys. Res. Solid Earth* 119 (4), 3767–3822. doi:10.1002/2013jb010762
- Wang, Y., Wang, Y., Schoenbohm, L. M., Zhang, P., Zhang, B., Sobel, E. R., et al. (2020). Cenozoic Exhumation of the Ailaoshan-Red River Shear Zone: New Insights from Low-temperature Thermochronology. *Tectonics* 39, e2020TC006151. doi:10.1029/2020tc006151
- Wang, Y., Wang, Y., Zhang, P., Schoenbohm, L. M., Zhang, B., Zhang, J., et al. (2019). Intracontinental Deformation within the India-Eurasia Oblique Convergence Zone: Case Studies on the Nantinghe and Dayingjiang Faults. *Geophysical Soc. America Bull.* 132, 850–862. doi:10.1130/B35338.1
- Wang, Y. Z. (2009). *Continental Deformation Models and Their Application to Eastern Tibetan Plateau (In Chinese with English Abstract)*, PhD Thesis. Beijing: Institute of Geology, China Earthquake Administration.
- Wang, Y., Zhang, B., Schoenbohm, L. M., Zhang, J., Zhou, R., Hou, J., et al. (2016). Late Cenozoic Tectonic Evolution of the Ailao Shan-Red River Fault (SE Tibet): Implications for Kinematic Change during Plateau Growth. *Tectonics* 35 (8), 1969–1988. doi:10.1002/2016tc004229
- Weldon, R., Sieh, K., Zhu, C., Han, Y., and Robinson, S. (1994). “Slip Rate and Recurrence Interval of Earthquakes on the Hong He (Red River) Fault, Yunnan, P.R.C.” in *International Workshop on Seismotectonics and Seismic Hazard in SE Asia* (Hanoi: UNESCO), 244–248.
- Wells, D. H., and Coppersmith, K. J. (1994). New Empirical Relationships Among Magnitude, Rupture Length, Rupture Width, Rupture Area, and Surface Displacement. *Bull. Seismological Soc. America* 84 (4), 974–1002.
- Ye, W. H., Xu, X. W., and Wang, L. M. (1996). Quantitative Relationship between Surface Rupture Parameter, Earthquake Magnitude and Recurrence Interval for Surface Rupturing-Earthquake in West China (In Chinese with English Abstract). *Seismology Geology*. 18 (1), 37–44.
- York, D., Evensen, N. M., Martí nez, M. L., and De Basabe Delgado, J. (2004). Unified Equations for the Slope, Intercept, and Standard Errors of the Best Straight Line. *Am. J. Phys.* 72 (3), 367–375. doi:10.1119/1.1632486
- Yu, W. X., Hou, X. Y., Zhou, R. Q., Chai, T. J., and Gu, Y. S. (1991). Characteristic Surface Ruptures of Langcang-Gengma Earthquake (In Chinese with English Abstract). *Jouranal Seismology Res.* 14 (3), 203–214.
- Zhu, Y. X., Li, P., and Ren, J. W. (1994). Activity of Nantinghe Fault Zone and its Paleoeearthquake Events (In Chinese with English Abstract). *Earthquake Res. China* 10 (4), 347–356.

Conflict of Interest: The authors declare that the research was conducted in the absence of any commercial or financial relationships that could be construed as a potential conflict of interest.

Publisher’s Note: All claims expressed in this article are solely those of the authors and do not necessarily represent those of their affiliated organizations, or those of the publisher, the editors and the reviewers. Any product that may be evaluated in this article, or claim that may be made by its manufacturer, is not guaranteed or endorsed by the publisher.

Copyright © 2022 Shi, He, Liu, Wei and Sun. This is an open-access article distributed under the terms of the Creative Commons Attribution License (CC BY). The use, distribution or reproduction in other forums is permitted, provided the original author(s) and the copyright owner(s) are credited and that the original publication in this journal is cited, in accordance with accepted academic practice. No use, distribution or reproduction is permitted which does not comply with these terms.